PCCP

Accepted Manuscript

ROYAL SOCIETY OF CHEMISTRY

www.rsc.org/pccp

Structure Prediction of the Solid Forms of Methanol: An Ab Initio Random Structure Searching Approach

Tzu-Jen Lin, Cheng-Rong Hsing, Ching-Ming Wei and Jer-Lai Kuo

Institute of Atomic and Molecular Sciences, Academic Sinica, Taipei, 10617, Taiwan

Abstract

Liquid methanol and methanol clusters have been comprehensively studied to reveal their local structure and hydrogen bond networks. However, our understanding of the crystal forms of methanol is rather limited. The known crystal structures of solid methanol, α, β, and γ, are composed of infinite hydrogen bond chains in their unit cell. The structural diversity of solid methanol is much less than that of liquid methanol, in which both chain and ring structures exist and have been confirmed by experiments. In this study, we employed ab initio random structure searching (AIRSS) to study possible solid methanol structures. AIRSS predicted known solid methanol phases as well as various ring structures that have not been considered. A new possible candidate structure for the δ phase was also discovered. The relative stability of known solid methanol phases and our newly discovered structures were also investigated through dispersion corrected density functional theory. The density functional calculation provides reliable phase transition pressures between the known phases and the searched structures compared with experimental suggestions. In addition, the simulation result indicated that CH···O hydrogen bonds play a major role in stabilizing the methanol crystals under high pressures.

1. Introduction

Methanol is a crucial substance that is required for industrial applications, planetary evolution, and high-pressure experiments. Additionally, its use as an antifreezer to prevent clathrate hydrate blockages in oil and gas pipelines is well-established.[1] In planetary evolution, methanol is considered a critical component of the subsurface oceans on Titan.[2] The amount of methanol affects outer ice shell dynamics on icy planets because it alters the rheological properties of the primordial ocean. Methanol is also a common solvent used to create solvates in the pharmaceutical industry and new organic relaxor ferroelectric materials.[3-7] In high-pressure experiments, neat methanol or a 4:1 methanol–ethanol solution is widely employed as a pressure-transmitting medium up to 10 GPa.[8]

In addition to its various applications, methanol is scientifically crucial because it is a simple and critical model for studying the hydrogen bonding network. Methanol can be considered a counterpart of water when one hydrogen atom of a water molecule is replaced with the methyl group. Therefore, the oxygen atom in a methanol molecule is a single hydrogen bond donor and acceptor, whereas the oxygen atom in a water molecule is a double hydrogen bond donor and acceptor. The hydrogen bonding network of methanol should be less complicated than that of water. For last decades, neat and protonated methanol clusters have been extensively studied experimentally and theoretically to understand the local structure of liquid methanol and its hydrogen bonding networks. In the gas phase, three methanol molecules form a ring structure, which is considered the basic motif, and large methanol clusters are the expansion of the ring structure examined through infrared (IR studies.[9, 10] Protonated methanol clusters $[H^+(MeOH)_n]$ in the gas phase have also been examined, and because of the extra proton, they have a more complex hydrogen bonding network than their neutral counterparts do. Bicyclic structures have been discovered for n = 7 and 8 of $[H^+(MeOH)_n]$.[11, 12] The local structure of liquid methanol consists of a chain structure of up to 10 methanol molecules with an average of six molecules, as suggested by neutral diffraction experiments.[13] Cyclic hexamer, linear trimer, and tetramer chains were discovered by Sarkar and Tanaka.[14, 15] Guo et al used X-ray emission to propose that hydrogen bonded chains and six/eight-member ring are predominantly persist with equal abundance in pure liquid methanol.[16] Many theoretical studies have been conducted on methanol clusters with sizes ranging from 2 to 20.[17-20] In these theoretical studies, various types of clusters, such as chain, ring, folded ring, and stacked ring, have been examined, reflecting the inherent diversity of the local structure of liquid methanol.

Compared with gas and liquid phases, knowledge of the solid structure of methanol is limited. In addition, methanol crystals do not receive the considerable attention that other hydrogen-rich molecular crystals such as methane, ammonia, and ice do.[21-24] Only three phases of solid methanol, namely α, β, and γ, are mentioned in the literature.[25-29] α and β phases are discovered under ambient pressures, and both have four methanol molecules in their orthorhombic unit cells. The α phase was revealed at a temperature below 160 K with the space group $P2_12_12_1$. The hydrogen bond chains are linear, puckered, and antiparallel one another. The β phase exists between the melting temperatures 175 K and 156 K and was initially accepted to possess *Cmcm* symmetry,[30] but its structure was later determined to have $Cmc2_1$ symmetry.[28] The structure of the β phase resembles that of α phase, and it is also composed of infinite hydrogen bond chains. The difference between α and β phases is the packing among OH···O hydrogen bond chains. The hydrogen bond chains are tilted toward one another in the α phase but not in the β phase (Fig. 1). Methanol easily forms a glassy state under pressure and the results of methanol crystallization under high pressure were not conclusive. Brugmans and Vos demonstrated that methanol formed crystals between 5 and 10 GPa, and the nucleation rate was highest at 7 GPa. The crystals had facet-like morphology that was recognized through optical microscopy.[31] The γ phase is the only known high pressure phase of solid methanol that has structural information mentioned in the literature.[26] The authors obtained a single γ phase crystal by first pressurizing liquid methanol up to 7 GPa to form crystallites followed by cycling the temperature above the melting temperature at a high pressure to reduce the number of grains, and the crystal was stable above 4 GPa.[26] The structure had triclinic $\overline{P1}$ symmetry with six methanol molecules in the unit cell and two infinite antiparallel hydrogen bond chains, as displayed in Fig. 1. The irregular hydrogen bond lengths are the primary feature of this structure, suggesting that hydrogen bonds between methanol molecules are strained at this high pressure phase.

In addition to the aforementioned known solid methanol phases, some studies have suggested the presence of a new crystalline methanol phase. Ferry[32] discovered a metastable phase through vapor pressure measurement; however, this result was challenged by Galvez[29] who, according to IR spectroscopic data, suggested that this metastable phase was only a combination of α and β phases. Gromnitskaya *et al*[33] used an ultrasonic technique to study the phase diagram of methanol at a temperature range of 90–290 K and a pressure range of up to 1.2 GPa. Because the pressure range was narrow, the authors did not find any new phases of methanol at high pressure, whereas the study suggests low-density and high-density transitions in liquid methanol at 230–250 K and 0.2–0.6 GPa. Kondrin *et al*[34] employed

dielectric spectroscopy to study the phase diagram of methanol at a pressure of up to 6 GPa and a temperature range of 100–360 K. The authors confirmed the presence of the γ phase and suggested a new phase called the δ phase that was stable at pressures of >1.2 GPa and temperatures of <270 K. In addition, the presence of a new phase between 3.4 and 3.7 GPa and at 260–280 K was also proposed, and these new structures could be transformed from the β phase. Although these studies indicated the possibility of new solid phases of methanol at high pressures, structure verifications have not been conducted. Raman, IR, ultrasonic wave, or nuclear magnetic resonance studies have been performed to determine the crystal structure of solid methanol under high pressures, but the conclusions remain unclear.[35-38]

Algorithms regarding to crystal structure prediction (CSP) are useful to fill the gap caused by missing structural verification data from experimental studies. To the best of our knowledge, a structure search for solid methanol has not been performed. Moreover, the known solid phases of methanol, α, β, and γ, are composed of infinite hydrogen bonds, and ring structures often observed in gas and liquid phases of methanol have never been considered in the solid phase. From a kinetic point of view, infinite hydrogen bond chains are more difficult to form than ring structures are. Ring structures formed in the liquid state could pack with one another and transform into crystals; however, infinite hydrogen bond chains can be easily destroyed if even a single methanol molecule is not aligned. Therefore, identifying new structures other than infinite hydrogen bond chains in the solid phase of methanol would be appealing. Many algorithms have been proposed for CSP, such as random searching,[39, 40] particle swarm optimization,[41, 42] and an evolutionary algorithm.[43-45] In this study, ab initio random structure searching (AIRSS) was performed to search for new solid methanol structures with the assistance of dispersion-corrected density functional methods.

2. Computational Details

In this section, we will address the computational method and the approach used in AIRSS. The performance of dispersion corrected functional is determined by the cohesive energy and the geometry parameter of OH···O hydrogen bond in α and β phases in section 2.1. The detail of AIRSS approach is addressed in section 2.2, and the method for predicting phase transition pressure of different phases is presented in the final section 2.3. All density functional theory (DFT)[46] calculations in this study were performed using the Vienna Ab initio Simulation Package.[47-50] The projector-augmented wave method was used.[51, 52] During a random search, the kinetic energy cutoff was set as 450 eV, and 600 eV was employed for the following energy–volume analysis, in which energy and force tolerance were set to 10^{-5} eV and 0.01 eV $Å^{-1}$, respectively. A 4 × 4 × 4 k-point grid for Brillouin zone sampling through the Monkhorst–Pack scheme was used.[53]

2.1 Choice of Exchange and Correlation Functional

Because of the presence of the methyl group in methanol molecules, dispersion-corrected functionals were used. Without the dispersion correction, the equilibrium volume of the α phase was 60% larger than the experimental values. For the energy–volume analysis, four types of dispersion-corrected (or included) functionals, optB86b,[54] optB88,[55] PBE-D3,[56] and PBE-D2,[57] were tested. optB86b and optB88 were modified on the basis of the van der Waals density functional (vdW-DF) proposed by Dion.[58] vdW-DF evaluates dispersion interactions according to electron density. In Grimme-type correction scheme, such as D2 and D3, empirical van der Waals interaction is added after self-consistent field calculations. The cohesive energies of α and β phases and methanol dimer are computed to test the performance of these dispersion-corrected functionals. Cohesive energy was calculated by subtracting equilibrium energy from the equation of state and that from a methanol molecule in the gas phase. The computed cohesive energy and experimental sublimation energy for α and β phases are listed in Table 1. Experimental sublimation enthalpies[32] were corrected back to zero temperature value for comparison.[59] Few studies have employed ab initio methods for computing the cohesive energy of solid methanol. Nagayoshi *et al*[60] used the MP2 method to compute the cohesive energy of a methanol crystal; its value has been listed in Table 1 for

comparison. We found that, compared with experimental data, computed cohesive energies were overestimated; however, the energy difference between α and β phases, which was approximately 20 meV per molecule according to various dispersion-corrected functionals, was consistent with experimental data. The cohesive energy computed by Nagayoshi *et al* differed substantially from experimental data. This could have resulted from the unrelaxed structures and the inclusion of only two-body energy in the calculations. We also examined the binding energy of methanol dimers obtained from the S66 database,[61] and all functionals used in this study displayed consistent overestimations. In addition, the trends of phase transition pressures predicted by these four functionals are consistent to one another displayed in Fig. S1. These functionals reproduce similar geometry parameter of OH···O hydrogen bond of known methanol crystals. The computed OH···O hydrogen bond lengths of α phase are 1.63 Å which is 0.1 Å shorter than experimental study on deuterated samples at 15 K. Similar results were obtained by Galvez et al.[29] These shorten hydrogen bonds correspond to the overestimated cohesive energy in Table 1. Accordingly, the current DFT approach slightly overestimates the strength of OH···O hydrogen bonds. The computed bond angle of OH···O hydrogen in α phase is 179.8 degree, which is 4° higher than the value found in deuterated sample at 15K and shows great linearity of the hydrogen bond. In the crystallographic data (CIF file) provided by Boese et al[28], OH···O hydrogen bond in β phase is 1.88 Å and the bond angle is 166°. The computed bond lengths and angles about 1.62 Å and 176° for β phase respectively. This large deviation to experimental data is because of overestimation of the OH···O hydrogen bond interaction aforementioned in α phase and not including temperature factor in DFT calculations leading to similar geometry parameter of OH···O hydrogen bonds as low-temperature α phase. Nevertheless, the OH···O hydrogen bonds in β phase exhibit less linearity than α phase. The aim of this study is to understand the relative stability of different crystal structures and changes of the hydrogen bonds under various pressures. Although the computed geometry parameters of OH···O hydrogen bonds do not fully match with experiments, we still speculate that DFT calculations can still capture the change of hydrogen bonds when methanol crystals under pressures.

2.2 Ab Initio Random Structure Searching

AIRSS has been successfully used for predicting stable and metastable structures of crystals, clusters, and point defects in solids. Because many high-energy states can be discovered through AIRSS, experimental information, particularly chemical and structure

information, can be employed as constraints to increase the efficiency of searching local minimums.[40]

In this study, the first constraint was the system size. According to the known α, β, and γ phases, we limited the system size to four and six methanol molecules in the unit cells. The second constraint was the cell parameter. The experimentally determined cell parameters of the α phase (a = 4.8728 Å, b = 4.6411 Å, c = 8.8671 Å, $\alpha = \beta = \gamma = 90°$), β phase ($a$ = 6.43 Å, b = 7.24 Å, c = 4.67 Å, $\alpha = \beta = \gamma = 90°$), and γ phase ($a$ = 7.67 Å, b = 4.4101 Å, c = 7.199 Å, α = 88.1°, β = 102.89°, γ = 93.85°)[25, 26, 30] can be an appropriate initial selection for the random search. Therefore, the cell parameters of α and β phases were utilized for systems containing four methanol molecules, and those of the γ phase were used for systems containing six methanol molecules. The third constraint was the space group. We also employed the space groups determined through experiments as constraints during the random search. The space groups of α ($P2_12_12_1$) and β ($Cmc2_1$ or $Cmcm$) phases belonged to higher symmetry groups, indicating that, compared with that in lower symmetry groups, the search in the configuration space was severely limited. By using the space group of α and β phases for the cell containing four methanol molecules, the random search quickly converged to the crystal structure of α and β phases determined through experiments. Therefore, the random search was directed toward the lower symmetry space group, such as inversion center symmetry ($\overline{P1}$), which is identified in the γ phase or even without symmetry (P1). When methanol molecules were inserted into the unit cell, each methanol molecule was considered a rigid body. Because methanol does not possess internal degrees of freedom, which drastically alter its conformation, the rigid body approximation is reasonable. After placing a methanol molecule into the unit cell, the entire molecule was then randomly rotated. The same process was performed for the next methanol molecule. After creating methanol crystal structures, constant volume optimizations were performed through PBE-D3 functional.[56]

More than 600 structures were searched, their energies were sorted from lowest to highest, and the structures with P1 and $\overline{P1}$ symmetry were placed in the same pool for comparison. Figures 2(a) and (b) display the relative energy ranking for unit cells containing four methanol molecules by using the lattice parameters of α and β phases, respectively. From the search constrained by the lattice parameter of α phase, the searched structures were composed of the infinite hydrogen bond chain structure. No new class of structure was found under this search constraint. The structure with the lowest relative energy possessed the α phase structure. At relative energies between 5 and 20 meV per molecule, crystal structures

resembling the β phase structure were also discovered. This result indicated the reliability of our search strategy because it could predict experimentally determined crystal structures. Beyond the region of 20 meV per molecule, the crystal structures exhibited highly unfavorable packing among methanol molecules.

When the search was constrained using the lattice parameter of the β phase, two new classes of structures were discovered: 4R and 4S (Fig. 3). 4R is a four-membered ring structure composed of four OH···O hydrogen bonds. Moreover, the four methyl groups are in an up–up–down–down configuration to retain the $\overline{P1}$ symmetry. 4S can be considered a ring-opening structure of 4R. One side of the four-membered ring is open, and the network is similar to a spoon. 4S has one infinite hydrogen bond chain, which points in one direction, resulting in non-zero dipole moments. Therefore, in the subsequent simulation, we doubled the cell size and compelled the other hydrogen bond chains to point in opposite directions to cancel the dipole moment. β phase and 4S structures had the lowest energy, and 4S was also dominant in the region where the relative energy was less than 25 meV per molecule [Fig. 2(b)]. β-like structures were also sporadically discovered in the same region as 4S was. Because these structures were similar to the known β phase, we did not consider them for further analysis. Again, the results demonstrated that our random search strategy was effective because it could locate crystal structures discovered in experiments. 4R structures were distributed in the plateau region between 25 and 30 meV per molecule [Fig. 2(b)].

The relative energy ranking for the crystal containing six methanol molecules with P1 and $\overline{P1}$ symmetry is displayed in Fig. 2(c). No dominating structures were found in this search, a result that differs from that of the search for the crystal containing four methanol molecules. The structure possessing the lowest energy was the γ phase, and the energy was considerably lower than that of the structure having the second lowest energy by at least 33 meV per molecule. This is because during AIRSS, we employed the cell parameter of the γ phase as a constraint. The structure having the second lowest energy was a γ-like structure with P1 symmetry and was tentatively called δ′ (Fig. 3) because it could be a candidate for the δ phase in the later discussion section. In the subsequent energy–volume scan calculation, the energy of δ′ was lower in the γ phase by 10 meV per molecule at 4 GPa. Therefore, we examined structures having energy within 40 meV per molecule with respect to δ′. From the structural perspective, the δ′ phase was similar to the γ phase, and both were composed of two antiparallel infinite hydrogen bond chains in their unit cell. The difference between δ′ and γ phases was the packing of methyl groups. In this regard, the δ′ phase can be considered

a symmetry-break form of the γ phase. New types of structures, which were never considered in the solid state of methanol, such as a six-membered ring (6R) and four-membered ring with two outsider methanol molecules (4R2S) were also discovered in this energy scope. Both 6R and 4R2S possess the $\overline{P1}$ symmetry, and their structures are presented in Fig. 3. In 6R, three methyl groups are above the ring plane, and the other three are below the plane to fit the $\overline{P1}$ symmetry. Similar trends were also observed in 4R2S where four methyl groups in the four-membered ring were in an up–up–down–down configuration. Some structures similar to the γ phase with $\overline{P1}$ symmetry were also identified, and they also displayed differences in the orientation of methyl groups similar to those observed in δ′.

2.3 Pressure–Enthalpy Analysis

In energy–volume curve calculations, cell parameters and atomic positions were relaxed for a given volume. The initial crystal structures of α-, β-, and γ-phase methanol were obtained from of previous XRD studies. .[25, 26, 28] From the searched structures, 4S, 4R, 4R2S, 6R, and δ′ structures with the lowest energy were selected for analysis. For each structure, the volume was extended to up to 20% more than the equilibrium volume and was compressed to 35% less than the equilibrium volume. Changes in the volume were created using a step size of 3%. The energy–volume curves were then fitted to the Vinet exponential equation of state, which was validated for solids under a broad range of pressures.[62, 63] Theoretically, the phase transition pressure can be obtained by the common tangent of the energy–volume curves[64, 65]; however, the slopes cannot be predicted accurately. Alternatively, the transition pressure can be computed by Gibbs free energy at 0 K where it is equal to enthalpy, which is the internal energy plus the product of the pressure and volume ($P \cdot V$) of the system. In this study, the highest pressure used was only 10 GPa, and $P \cdot V$ scarcely contributed to the total enthalpy. Using the equation of state, pressure–enthalpy curves were obtained, and the curves were fitted to a polynomial with power 4 for comparing relative enthalpy among different structures at various pressures. When the relative enthalpies of two structures are nearly zero at a given pressure, the phase transition pressure can be identified.[66-69]

3. Results and Discussion

In this section, we will discuss the relative enthalpy of methanol crystal structures including found in AIRSS and known phases. We will first discuss the relative stability at

zero pressure in section 3.1 and under pressures in section 3.2. The role of OH···O and CH···O hydrogen bonds will be examined. In section 3.3, we will determine the phase transition pressure of different structures based on the computed pressure-enthalpy curves and correlate the result with experimentally suggested phase diagram of methanol.

3.1 Relative Enthalpy at Zero Pressure

The relative enthalpies of selected searched and known structures of solid methanol at various pressures are displayed in Fig. 4, in which the β phase is employed as a reference because it is stable in wide range of pressures and temperatures observed in experiments.[34] Information regarding the selected OH···O and CH···O hydrogen bonds of all structures is listed in Table 2. At zero pressure, the α phase had the lowest enthalpy among all the structures. The lowest enthalpy was attributed to the short and linear OH···O hydrogen bonds (1.62 Å and 179.8°) and three CH···O hydrogen bonds per methanol molecule, which is also the highest number of hydrogen bonds for a structure among all the structures at zero pressure. The enthalpies of 4S and β-phase structures were more than 20 meV per molecule more than that of the α-phase structure at zero pressure. The OH···O hydrogen bond lengths of 4S and β-phase structures were similar to that of the α phase structure; however, some OH···O hydrogen bonds in 4S and β-phase structures were slightly less linear (175 ± 1°) than that of the α-phase structure. More crucially, the number of CH···O hydrogen bonds in the 4S and β-phase structures, 1.75 and 1.0, respectively, was less than that of the α-phase structure.

The relative enthalpy of δ′ was lower than that of the γ phase by approximately 30 meV per molecule at zero pressure because the OH···O hydrogen bond length of δ′ (1.67 Å) was shorter than that of γ (1.72–1.75 Å), and the number of CH···O hydrogen bonds per molecule in δ′ (1.0) was higher than that in the γ phase (0.5). 4R and 6R had similar relative enthalpies, which were higher by 15–25 meV per molecule than those of the β-phase structure at zero pressure. Their OH···O hydrogen bond lengths were similar (1.65 ± 0.02 Å) and were slightly longer than those of the β-phase structure. Nevertheless, the OH···O hydrogen bond angles in 4R (approximately 170°) were less linear than those in the β-phase structure. Although 6R had linear OH···O hydrogen bonds (approximately 175°) equal to those in the β-phase structure, the crowded methyl groups in the six-membered ring (C···C distance was 3.5 Å) could partially offset the OH···O hydrogen bond interaction in the ring. The high relative enthalpy of 4R2S was attributed to weak hydrogen bonding (1.85 Å) between the four-membered ring and two outsider methanol molecules. In addition, energy-unfavorable packing between the two outsider methanol molecules contributed to the high relative enthalpy, as displayed in Fig. S3.

3.2 Relative Enthalpy Under Pressure

With increasing pressure, the relative enthalpies of the γ phase and δ′ decreased more rapidly than those of the other structures did. The OH···O hydrogen bond lengths of γ and δ′ decreased to 1.52 Å at 10 GPa, but the OH···O hydrogen bond angles remained constant at zero pressure, as displayed in Table 2. This suggests that the strength of OH···O hydrogen bonds in γ and δ′ increased during compression. Table 2 illustrates that the number of the CH···O hydrogen bond network increased rapidly for γ and δ′. When the pressure changed from 0 to 4.5 GPa, the number of CH···O hydrogen bonds per molecule increased from 0.5 to 3.5 and 1.0 to 3.67 in γ and δ′, respectively. Figure 5 schematically displays the increase in the CH···O hydrogen bond networks. The growth of CH···O hydrogen bonds in γ and δ′ was considerably higher than that of any other structure in this study. The building magnitude of OH···O hydrogen bonds and substantially increased CH···O hydrogen bond networks reduced the relative enthalpy of γ and δ′ faster than any other structure did between 0 and 4.5 GPa. Although the increase in the CH···O hydrogen bond network was limited in γ and δ′ after 4.5 GPa, the magnitude of OH···O hydrogen bonds increased compared with those of the β phase, where the strength of the hydrogen bond decreased after 4.5 GPa, thereby reducing the relative enthalpy with respect to the β phase.

The relative enthalpies of 4R, 4R2S, and 6R gradually approached that of β under compression (Fig. 4). Their enthalpy difference was <10 meV per molecule when the pressure exceeded 3.5 GPa. Table 2 illustrates that the OH···O hydrogen bonds of 4R, 4R2S, and 6R were all reduced; however, their OH···O hydrogen bond angles displayed variations during compression. The OH···O hydrogen bond angles in the four-membered ring of 4R and 4R2S were approximately 170° with a change of <2° under compression. The OH···O hydrogen bonds between the four-membered ring and associated methanol molecules in 4R2S were distorted during compression. The OH···O hydrogen bond angles of 6R deviated considerably from 180° during compression. On the basis of the OH···O hydrogen bond information between these ring structures and the β phase at pressures between 0 and 4.5 GPa, the relative enthalpies of these ring structures should be parallel one another or gradually away that of the β phase, but this trend was not observed (Fig. 4). The CH···O hydrogen bond interaction causes the relative enthalpies of 4R, 4R2S, and 6R to be close to that of the β phase during compression. As displayed in Table 2, the growth of the CH···O network in the β phase was only 50% from 0 to 4.5 GPa. By contrast, the CH···O network in 4R, 4R2S, and

6R expanded by at least 2.3 times. Compared with the β phase, the increased CH···O interactions provided these ring structures extra stabilization energy. Because the increase in the CH···O network in the ring structures was less than that in γ and δ′, the relative enthalpies of the structures did not decrease as fast as those of γ and δ′ did. After 4.5 GPa, the increase in the rate of CH···O hydrogen bond formation decreased in these ring structures. Some of the OH···O hydrogen bond angles in 4R and 4R2S did not change considerably, in contrast to the deteriorating hydrogen bonds in the β phase when pressure exceeded 4.5 GPa. Consequently, the relative enthalpies of 4R and 4R2S decreased after 4.5 GPa with respect to the β phase. The decreasing rate of 6R was slower than that for the other ring structures when the pressure exceeded 4 GPa. This was because the crowed methyl groups caused a strong repulsion in 6R, which largely deteriorated the linearity of OH···O hydrogen bonds in the six-membered ring. At 10 GPa, the closest C···C distance was 3.6 Å in 4R and 3.0 Å in 6R.

The relative enthalpy versus pressure curve of 4S displays behavior that differs from that of the other structures in Fig. 4. Its relative enthalpy increased rapidly under compression and reached a plateau after 4.5 GPa regarding the β phase. Unexpectedly, the CH···O network increased rapidly from 0 to 4.5 GPa. We demonstrated that the increased CH···O network provided considerable stabilization energy when the crystal was being compressed. Therefore, the increased relative enthalpy must have been attributed to other factors. The increased relative enthalpy could be attributed to the distorted OH···O hydrogen bond angle displayed in Table 2. However, distorted hydrogen bonds cannot completely explain this observation because 6R also has a distorted OH···O hydrogen bond and an increased CH···O hydrogen bond network during compression with decreasing relative enthalpies with respect to the β phase. The rapidly increasing relative enthalpy of 4S between 0 and 4.5 GPa is attributed to the close O···O contact illustrated in Fig. 6. Because one side of the open-ring structure in 4S does not have the OH···O hydrogen bond, this side is easily compressed when pressure is applied. The O···O distance on this side is then reduced, and considerable repulsion is created because of the close contact between the two negatively charged atoms. The change of the O···O distance in 4R is also displayed in Fig. 6. The O···O distance decreased drastically from 3.79 Å at zero pressure to 3.51 Å at 4.5 GPa. The number of CH···O hydrogen bonds also increased considerably in 4S with respect to the β phase from 0 to 4.5 GPa. In this regard, the repulsive interactions between the two oxygen atoms were partially balanced by CH···O hydrogen bonds, enabling the relative enthalpy of 4S to reach the plateau region. After 4.5 GPa, the O···O distance did not considerably change, and the distance was 3.45 Å at 10 GPa, which was only 0.06 Å shorter than that at 4.5 GPa.

Considering that OH···O hydrogen bonds between 4S and the β phase gradually deteriorated beyond 4.5 GPa, the relative enthalpies between these two phases were expected to be similar to each other, as demonstrated in Fig. 4.

3.3 Predicted Phase Diagram

The phase diagram of solid methanol provided in Fig. 7 is based on the pressure–enthalpy curve in Fig. 4 and dielectric spectroscopy performed by Kondrin *et al*,[34] and the experimentally suggested phase diagram is presented in Fig. S4. The relative enthalpies of α and δ′ phases were less than 10 meV per molecule from 1.25 to 3 GPa. DFT calculation is suitable for low temperature conditions because no temperature factor is involved. In this regard, the phase boundary between α and δ′ phases was drawn from 1.25 to 3 GPa in the low temperature region. This predicted phase boundary was also close to the experimental measurements where the boundary ranged from 1.25 to 3.25 GPa. The relative enthalpies of δ′ and γ phases were close to each other when pressure exceeded 4 GPa. Accordingly, the region over 4 GPa with low temperature was denoted as "δ′ or γ," and a dashed line was drawn at the point exhibiting 4 GPa in Fig. 7 because we were unsure which phase would be dominant at this pressure range. In summary, the α phase transformed into the δ′ phase at the pressure range of 1.25 to 3 GPa, and the δ′ phase then transformed into the γ phase at 4 GPa at low temperature.

According to the computed pressure–enthalpy diagram in Fig. 4, the relative enthalpies between α and γ phases were less than 10 meV per molecule from 3 to 4.5 GPa; therefore, we labeled the region from 3 to 4.5 GPa between the α and γ phases as a grey region. This result is consistent with the speculation based on dielectric measurements.[34] Vega[70, 71] employed classical force fields to calculate the phase transition pressure between α and γ phases; however, the predicted phase transition pressure was approximately 10 GPa higher than the expected pressure. This is because classical force field cannot describe the interaction of methanol in the solid state well especially when the methanol crystals under compressions. No matter the intermolecular distances between methanol molecules are increased or reduced, the interaction parameter is fixed in classical force fields. On the contrary, the electron density distribution which governs interactions between molecules is obtained by self-consistent field method at a given intermolecular distance in DFT

calculations. Therefore, the interaction strengths between methanol molecules is distance dependent.

Because the predicted phase transition pressure between α and γ phases without the inclusion of temperature was nearly equal to that of the experimental study, this feature could be used to explain the phase transition between the β phase and other ring structures. When the pressure exceeded 3 GPa, the enthalpies of 4R, 6R, and 4R2S were similar to that of the β phase with a difference of less than 10 meV per molecule. This finding suggests that many new phases could be formed while pressurizing the β phase to more than 3 GPa. This computational result also supported "β-β′ transition" in the intermediate P–T region with pressures of 3.4–3.7 GPa and temperatures of 260–280 K observed by Kondrin *et al*[34] through dielectric spectroscopy. From a thermodynamic perspective, this explains why methanol is difficult to crystallize under pressures at room temperature because many ring structures may transform into one another. Because the relative enthalpies between ring structures and the β phase were similar after 3 GPa, we denoted "β or R" and drew a dashed line at 3 GPa in the high temperature region (Fig. 7). Although the 4S structure was not stable at a pressure of more than 3.5 GPa compared with the other structures, 4S had an enthalpy that was similar to that of the β phase at a low pressure (Fig. 4). 4S may be stable at low temperatures with pressures of <1 GPa. Therefore, we indicated 4S in the low temperature and pressure region of the β phase.

Kondrin *et al*[34] suggested that a δ phase with $P2_1/m$ symmetry exists in the lower temperature region than γ phase, and it contains eight methanol molecules in a unit cell. This suggestion lacked structure verification. In addition, the proposed $P2_1/m$ symmetry includes mirror planes, excluding the possibility of having antiparallel hydrogen chains and stable ring structures. The antiparallel chains and ring structures are the only two patterns that form a stable crystal according to the single–donor single–acceptor character of neutral methanol. Therefore, the searched structure, δ′ with P1 symmetry, is a more likely candidate for δ than the suggestion of Kondrin *et al*.[34]

4. Conclusions

AIRSS was performed to study the molecular crystal of methanol. Although some constraints were used during the search, the results revealed that the crystal forms of solid methanol exhibited rich structure diversity, in contrast to conventional knowledge. Several types of new ring structures, such as 4R, 6R, and 4R2S, were discovered, and they could be

obtained by pressurizing the β phase or liquid phase of methanol over 3 GPa. These structures differed greatly from known methanol crystal phases that are composed of infinite hydrogen bond chains. Ring structures have not been considered in the solid state of methanol, but their formation can reasonably be expected to be kinetically more accessible than chain structures because packing between the ring structures is much easier than aligning every methanol molecule along an extended distance. Very recent high-pressure experiments on liquid methanol by Hsieh and Chien[72] does not observe specific phase by using Raman spectroscopy. As mentioned in previous work done by Brugmans and Vos,[26, 31] to crystallize methanol from liquid state is not easy and needs many kinetic processes. In Hsieh and Chien's work, they only compress liquid method directly up to high pressures without introducing any other kinetic process. This could be the reason why they did not observe phase changes. An open-ring structure, 4S, was discovered, and it may coexist with the β phase at a low pressure and temperature. 4S became highly unstable when pressure was applied because of the close contact between two oxygen atoms without any hydrogen bonding between them. A possible candidate for the δ phase (δ′) was also identified, and δ′ had P1 symmetry with six methanol molecules in the unit cell. The crystal structure of δ′ resembled the γ phase with different arrangements of methyl groups. The phase transition pressure of α–δ′ transition was between 1.25 and 3 GPa, and δ′ could transform into γ at 4 GPa, as predicted by density functional calculations. Pressure–enthalpy analysis indicated that the CH···O hydrogen bond network played a major role in stabilizing the methanol crystal during pressurization. The considerably increased CH···O network stabilized γ and δ′ phases up to 10 GPa, and it also altered the enthalpy of the ring structures, causing the enthalpy to be close to that of the β phase during compression. If new phases of methanol exist at high pressures, then the crystal structure should be maximizing CH···O hydrogen bond interactions.

These newly identified structures could provide insights into the crystallization of liquid methanol under high pressure, which is still missing today. In addition, these structures are useful to future structure determinations. They can be used as input model to simulate diffraction pattern or IR/Raman spectrum to correlate with experiments. These newly identified structures are provided as Crystallographic Information File (CIF) in supporting information. The constrained AIRSS used in this study may also be applicable to other alkyl-monoalcohols, such as tertiary butyl alcohol, cyclobutanol, or phenol, to search possible structures under high pressures.[73-77] The low symmetry in δ′ and the structural diversity for the unit cell containing six methanol molecules suggest that more detailed structure searches

or algorithms, such as using the structures obtained through AIRSS followed by applying a generic algorithm to explore the complex potential energy surface, can be developed in the future.

Acknowledgments

This study was financially supported by various grants of Academia Sinica and the Ministry of Science and Technology of Taiwan (Grant: MOST102-2113-M-001-012-MY3 and MOST101-2113-M-001-023-MY3). We are grateful for the generous allocation of computational resources provided by the National Center for High-Performance Computing and Academia Sinica Computing Center.

Reference

1. K. Shin, K. A. Udachin, I. L. Moudrakovski, D. M. Leek, S. Alavi, C. I. Ratcliffe and J. A. Ripmeester, *Proceedings of the National Academy of Sciences*, 2013, **110**, 8437-8442.
2. D. Frédéric, M. Olivier, S.-V. Carmen and I. L. Jonathan, *The Astrophysical Journal*, 2010, **724**, 887.
3. P. A. W. Dean, M. Jennings, T. M. Houle, D. C. Craig, I. G. Dance, J. M. Hook and M. L. Scudder, *CrystEngComm*, 2004, **6**, 543-548.
4. S. L. Morissette, Ö. Almarsson, M. L. Peterson, J. F. Remenar, M. J. Read, A. V. Lemmo, S. Ellis, M. J. Cima and C. R. Gardner, *Advanced Drug Delivery Reviews*, 2004, **56**, 275-300.
5. P. Vishweshwar, J. A. McMahon, J. A. Bis and M. J. Zaworotko, *Journal of Pharmaceutical Sciences*, 2006, **95**, 499-516.
6. A. Olejniczak and A. Katrusiak, *CrystEngComm*, 2010, **12**, 2528-2532.
7. M. Anioła, A. Olejniczak and A. Katrusiak, *Crystal Growth & Design*, 2014, **14**, 2187-2191.
8. S. Klotz, J. C. Chervin, P. Munsch and G. L. Marchand, *Journal of Physics D: Applied Physics*, 2009, **42**, 075413.
9. H.-L. Han, C. Camacho, H. A. Witek and Y.-P. Lee, *The Journal of Chemical Physics*, 2011, **134**, 144309.
10. T. Kobayashi, R. Shishido, K. Mizuse, A. Fujii and J.-L. Kuo, *Physical Chemistry Chemical Physics*, 2013, **15**, 9523-9530.
11. T. Hamashima, Y.-C. Li, M. C. H. Wu, K. Mizuse, T. Kobayashi, A. Fujii and J.-L. Kuo, *The Journal of Physical Chemistry A*, 2013, **117**, 101-107.
12. J.-L. Kuo, A. Fujii and N. Mikami, *The Journal of Physical Chemistry A*, 2007, **111**, 9438-9445.
13. T. Yamaguchi, K. Hidaka and A. K. Soper, *Molecular Physics*, 1999, **96**, 1159-1168.
14. Y. Tanaka, N. Ohtomo and K. Arakawa, *Bulletin of the Chemical Society of Japan*, 1985, **58**, 270-276.
15. S. Sarkar and R. N. Joarder, *The Journal of Chemical Physics*, 1993, **99**, 2032-2039.
16. J. H. Guo, Y. Luo, A. Augustsson, S. Kashtanov, J. E. Rubensson, D. K. Shuh, H. Ågren and J. Nordgren, *Physical Review Letters*, 2003, **91**, 157401.
17. S. L. Boyd and R. J. Boyd, *Journal of Chemical Theory and Computation*, 2007, **3**, 54-61.
18. M. M. Pires and V. F. DeTuri, *Journal of Chemical Theory and Computation*, 2007, **3**, 1073-1082.
19. S. Kazachenko, S. Bulusu and A. J. Thakkar, *The Journal of Chemical Physics*, 2013, **138**, 224303.

20. G. Matisz, W. M. F. Fabian, A.-M. Kelterer and S. Kunsági-Máté, *Journal of Molecular Structure: THEOCHEM*, 2010, **956**, 103-109.
21. R. Bini and G. Pratesi, *Physical Review B*, 1997, **55**, 14800-14809.
22. A. D. Fortes, J. P. Brodholt, I. G. Wood and L. Vočadlo, *The Journal of Chemical Physics*, 2003, **118**, 5987-5994.
23. O. Kambara, K. Takahashi, M. Hayashi and J.-L. Kuo, *Physical Chemistry Chemical Physics*, 2012, **14**, 11484-11490.
24. B. Santra, J. Klimeš, A. Tkatchenko, D. Alfè, B. Slater, A. Michaelides, R. Car and M. Scheffler, *The Journal of Chemical Physics*, 2013, **139**, 154702.
25. B. H. Torrie, S. X. Weng and B. M. Powell, *Molecular Physics*, 1989, **67**, 575-581.
26. D. R. Allan, S. J. Clark, M. J. P. Brugmans, G. J. Ackland and W. L. Vos, *Physical Review B*, 1998, **58**, R11809-R11812.
27. B. H. Torrie, O. S. Binbrek, M. Strauss and I. P. Swainson, *Journal of Solid State Chemistry*, 2002, **166**, 415-420.
28. M. T. Kirchner, D. Das and R. Boese, *Crystal Growth & Design*, 2008, **8**, 763-765.
29. Ó. Gálvez, B. Maté, B. Martín-Llorente, V. J. Herrero and R. Escribano, *The Journal of Physical Chemistry A*, 2009, **113**, 3321-3329.
30. K. J. Tauer and W. N. Lipscomb, *Acta Crystallographica*, 1952, **5**, 606-612.
31. M. J. P. Brugmans and W. L. Vos, *The Journal of Chemical Physics*, 1995, **103**, 2661-2669.
32. S. Lucas, D. Ferry, B. Demirdjian and J. Suzanne, *The Journal of Physical Chemistry B*, 2005, **109**, 18103-18106.
33. E. L. Gromnitskaya, O. V. Stal'gorova, O. F. Yagafarov, V. V. Brazhkin, A. G. Lyapin and S. V. Popova, *Jetp Lett.*, 2004, **80**, 597-601.
34. M. V. Kondrin, A. A. Pronin, Y. B. Lebed and V. V. Brazhkin, *The Journal of Chemical Physics*, 2013, **139**, 084510.
35. J. F. Mammone, S. K. Sharma and M. Nicol, *The Journal of Physical Chemistry*, 1980, **84**, 3130-3134.
36. J. M. Zaug, L. J. Slutsky and J. M. Brown, *The Journal of Physical Chemistry*, 1994, **98**, 6008-6016.
37. R. A. Eaton, Y. N. F. Yuan and A. Anderson, *Chemical Physics Letters*, 1997, **269**, 309-313.
38. T. Okuchi, G. D. Cody, H.-k. Mao and R. J. Hemley, *The Journal of Chemical Physics*, 2005, **122**, 244509.
39. C. J. Pickard and R. J. Needs, *physica status solidi (b)*, 2009, **246**, 536-540.
40. J. P. Chris and R. J. Needs, *Journal of Physics: Condensed Matter*, 2011, **23**, 053201.
41. Y. Wang, J. Lv, L. Zhu and Y. Ma, *Physical Review B*, 2010, **82**, 094116.
42. J. Lv, Y. Wang, L. Zhu and Y. Ma, *The Journal of Chemical Physics*, 2012, **137**, 084104.
43. A. R. Oganov and C. W. Glass, *The Journal of Chemical Physics*, 2006, **124**, 244704.
44. A. R. Oganov, A. O. Lyakhov and M. Valle, *Accounts of Chemical Research*, 2011, **44**, 227-237.
45. A. O. Lyakhov, A. R. Oganov, H. T. Stokes and Q. Zhu, *Computer Physics Communications*, 2013, **184**, 1172-1182.
46. P. Hohenberg and W. Kohn, *Physical Review*, 1964, **136**, B864-B871.
47. G. Kresse and J. Hafner, *Physical Review B*, 1993, **47**, 558-561.
48. G. Kresse and J. Hafner, *Physical Review B*, 1994, **49**, 14251-14269.
49. G. Kresse and J. Furthmüller, *Computational Materials Science*, 1996, **6**, 15-50.
50. G. Kresse and J. Furthmüller, *Physical Review B*, 1996, **54**, 11169-11186.
51. P. E. Blöchl, *Physical Review B*, 1994, **50**, 17953-17979.
52. G. Kresse and D. Joubert, *Physical Review B*, 1999, **59**, 1758-1775.
53. H. J. Monkhorst and J. D. Pack, *Physical Review B*, 1976, **13**, 5188-5192.
54. J. Klimeš, D. R. Bowler and A. Michaelides, *Physical Review B*, 2011, **83**, 195131.
55. K. Jiří, R. B. David and M. Angelos, *Journal of Physics: Condensed Matter*, 2010, **22**, 022201.

56. S. Grimme, J. Antony, S. Ehrlich and H. Krieg, *The Journal of Chemical Physics*, 2010, **132**, 154104.
57. S. Grimme, *Journal of Computational Chemistry*, 2006, **27**, 1787-1799.
58. M. Dion, H. Rydberg, E. Schröder, D. C. Langreth and B. I. Lundqvist, *Physical Review Letters*, 2004, **92**, 246401.
59. A. Gavezzotti, *Modelling and Simulation in Materials Science and Engineering*, 2002, **10**, R1.
60. K. Nagayoshi, K. Kitaura, S. Koseki, S. Re, K. Kobayashi, Y.-K. Choe and S. Nagase, *Chemical Physics Letters*, 2003, **369**, 597-604.
61. J. Řezáč, K. E. Riley and P. Hobza, *Journal of Chemical Theory and Computation*, 2011, **7**, 2427-2438.
62. P. Vinet, J. Ferrante, J. R. Smith and J. H. Rose, *Journal of Physics C: Solid State Physics*, 1986, **19**, L467.
63. P. Vinet, J. R. Smith, J. Ferrante and J. H. Rose, *Physical Review B*, 1987, **35**, 1945-1953.
64. E. Whalley, *The Journal of Chemical Physics*, 1984, **81**, 4087-4092.
65. J. L. Aragones, E. G. Noya, J. L. F. Abascal and C. Vega, *The Journal of Chemical Physics*, 2007, **127**, 154518.
66. J. Feng, W. Grochala, T. Jaroń, R. Hoffmann, A. Bergara and N. W. Ashcroft, *Physical Review Letters*, 2006, **96**, 017006.
67. B. D. Malone and M. L. Cohen, *Physical Review B*, 2012, **85**, 024116.
68. Y.-L. Li, W. Luo, Z. Zeng, H.-Q. Lin, H.-k. Mao and R. Ahuja, *Proceedings of the National Academy of Sciences*, 2013, **110**, 9289-9294.
69. W. Xiaoli, T. Fubo, W. Lin, J. Xilian, D. Defang, H. Xiaoli, L. Bingbing and C. Tian, *New Journal of Physics*, 2013, **15**, 013010.
70. D. Gonzalez Salgado and C. Vega, *The Journal of Chemical Physics*, 2010, **132**, 094505.
71. D. Gonzalez-Salgado, A. Dopazo-Paz, P. Gomez-Alvarez, J. M. Miguez and C. Vega, *The Journal of Physical Chemistry B*, 2011, **115**, 3522-3530.
72. W.-P. Hsieh and Y.-H. Chien, *Scientific Reports*, 2015, **5**, 8532.
73. D. R. Allan and S. J. Clark, *Physical Review B*, 1999, **60**, 6328-6334.
74. D. R. Allan, S. J. Clark, A. Dawson, P. A. McGregor and S. Parsons, *Acta Crystallographica Section B*, 2002, **58**, 1018-1024.
75. D. R. Allan, S. Parsons and S. J. Teat, *Journal of Synchrotron Radiation*, 2001, **8**, 10-17.
76. P. A. McGregor, D. R. Allan, S. Parsons and S. J. Clark, *Acta Crystallographica Section B*, 2006, **62**, 599-605.
77. P. A. McGregor, D. R. Allan, S. Parsons and C. R. Pulham, *Acta Crystallographica Section B*, 2005, **61**, 449-454.

Fig. 1. Crystal structures of the known solid phases of methanol, α, β, and γ. OH···O hydrogen bonds are depicted using blue dashed lines. The hydrogen bonds of α and β phases are pointing inward and outward in relation to the diagram. In the γ phase, one hydrogen bond chain is pointing downward, and the other is pointing upward.

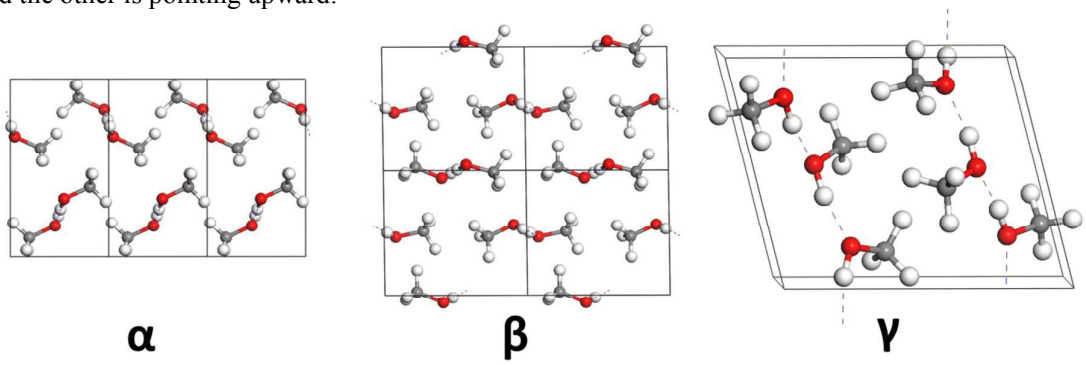

Table 1. Cohesive energies (meV/molecule) of α and β phases at zero pressure and methanol dimer from S66 database[60] calculated using different functionals. Experimental sublimation enthalpies were corrected back to zero temperature value.[58]

	PBE-D2	PBE-D3	optB86b	optB88	MP2	EXP or Benchmark
α	-582.20	-626.75	-675.88	-679.26	-650.40[a]	-511.51[b]
β	-562.05	-605.83	-659.41	-662.27	-494.30[a]	-485.64[b]
MeOH_S66	-276.5	-274.31	-266.76	-268.91	-254.56[c]	-251.49[d]

[a] Ref. 59 [b] Ref. 31 (vapor pressure measurements) [c] Ref. 60 (MP2/Complete basis set (CBS)) [d] Ref. 60 (CCSD(T)/CBS)

Fig. 2. Relative energy of structures obtained through AIRSS constrained by (a) the lattice parameter of the α phase with four methanol molecules, (b) the lattice parameter of the β phase with four methanol molecules, and (c) The lattice parameter of the γ phase with six methanol molecules. P1 and $\overline{\mathbf{P1}}$ space groups were implemented during the searches. The vertical axis is the energy in meV per molecule relative to the structure with the lowest energy on each search. The whole rank of the first 200 structures of (a) and (c) are presented in Fig. S2. A further discussion can be found in Section 2.1 of the main manuscript.

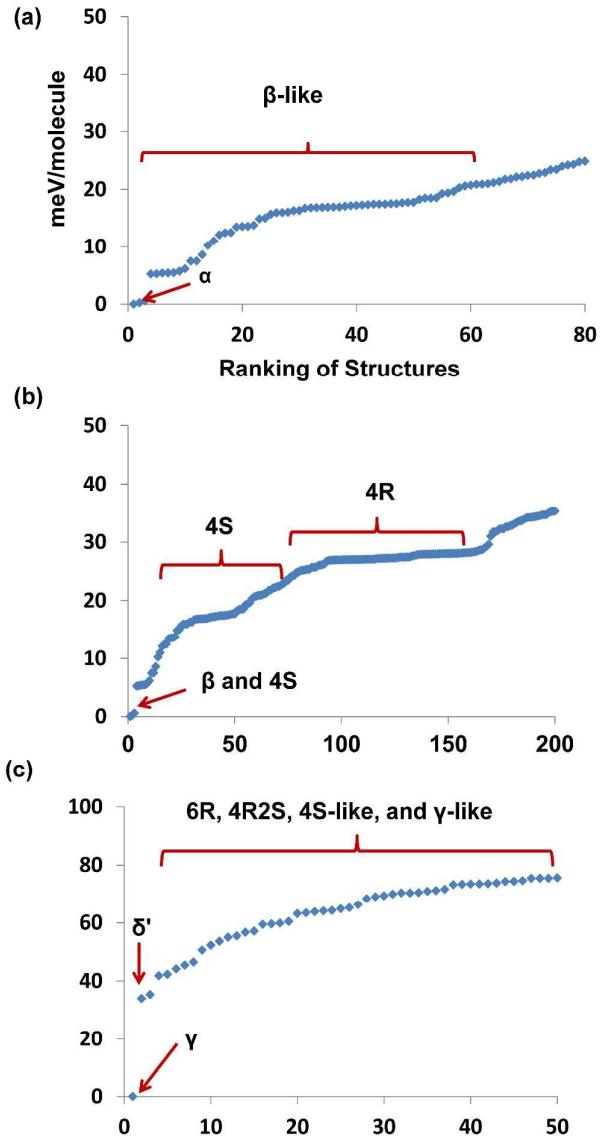

Fig. 3. Selected structures from the AIRSS with P1 and $\overline{\mathbf{P1}}$ symmetry. OH···O hydrogen bonds are depicted using blue dashed lines. 4S and δ′ have the P1 symmetry. 4R, 6R, and 4R2S have the $\overline{\mathbf{P1}}$ symmetry. The structure of the γ phase is also displayed here to demonstrate its similarity with δ′.

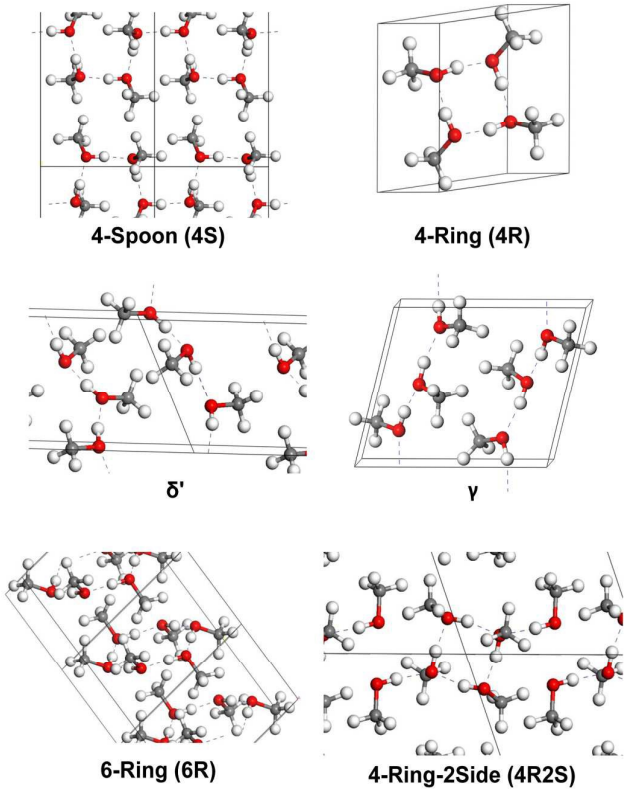

Fig. 4 Relative enthalpy–pressure curves from the selected searched and known crystal structures of methanol from 0 to 10 GPa by the optB86b functional. The vertical axis is the relative enthalpy (meV/molecule) with respect to the β phase, and the horizontal axis is pressure in GPa. (The relative enthalpy–pressure curves obtained using different DFT methods are compiled in Fig. S1.)

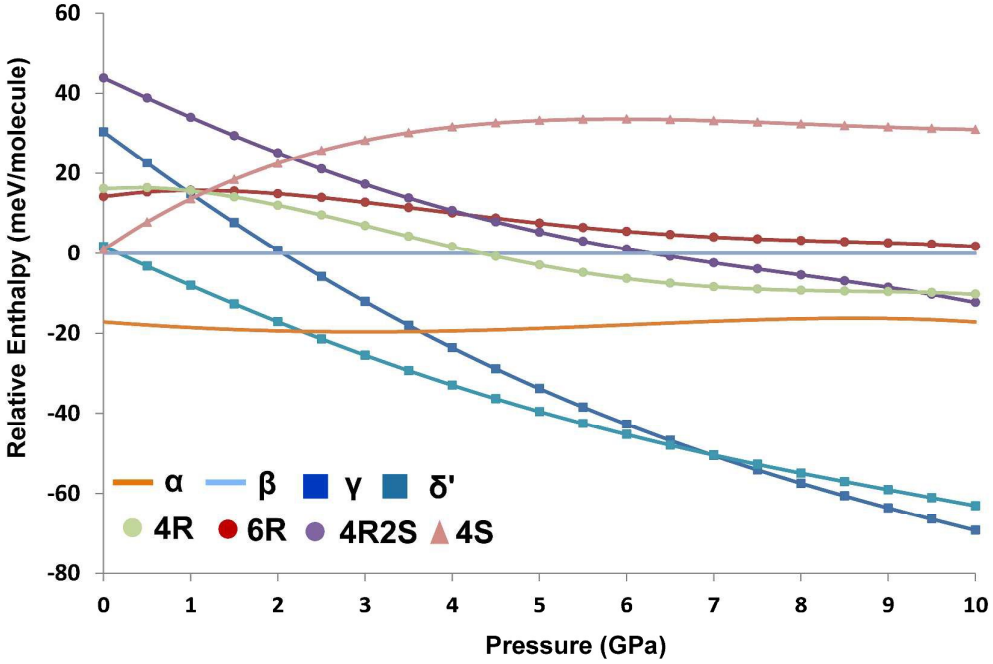

Table 2 Selected information of OH···O and CH···O bonds in known and searched structures of methanol crystals at 0, 4.5 and 10 GPa. OH···O hydrogen bond lengths are listed, and bond angle values (degrees) are provided in parentheses in the OH···O columns. The numbers of CH···O hydrogen bonds per molecule are listed in the CH···O columns. The first 2 OH···O hydrogen bonds in 4R2S were obtained from the ring structure. The criteria of these two hydrogen bonds are a bond length of <2.6 Å and a bond angle of >130°.

Pressure(GPa)	0		4.5		10	
Structure/Bonds	OH···O Å (degree)	CH···O #	OH···O Å (degree)	CH···O #	OH···O Å (degree)	CH···O #
α	1.63 (179.8)	3.0	1.55 (179.3)	3.0	1.59 (177.5)	4.0
β	1.62 (176.7) 1.61 (176.8) 1.62 (176.7) 1.64 (174.5)	1.0	1.54 (177.0) 1.54 (178.7) 1.55 (174.9) 1.57 (174.8)	1.5	1.52 (173.7) 1.52 (176.9) 1.52 (171.0) 1.53 (172.5)	2.25
4S	1.60 (174.8) 1.61 (178.8) 1.60 (174.7) 1.62 (178.9)	1.75	1.58 (170.4) 1.56 (167.8) 1.59 (169.7) 1.56 (167.0)	3.25	1.57 (169.8) 1.54 (162.0) 1.60 (164.2) 1.54 (159.7)	2.25
γ	1.72 (170.4) 1.73 (163.7) 1.71 (176.5)	0.5	1.63 (167.8) 1.62 (162.5) 1.60 (176.7)	3.5	1.55 (167.1) 1.53 (163.6) 1.52 (176.3)	3.83
δ’	1.67 (171.5) 1.67 (173.3) 1.67 (168.8)	1.0	1.59 (170.0) 1.58 (171.1) 1.57 (166.1)	3.67	1.52 (168.8) 1.53 (170.0) 1.49 (165.9)	4.33
4R	1.67 (168.1) 1.65 (170.6)	0.5	1.59 (168.0) 1.61 (169.7)	2.50	1.52 (166.7) 1.55 (171.1)	3.0
4R2S	1.66 (167.8) 1.73 (167.9) 1.85 (170.0)	0.67	1.54 (169.3) 1.62 (167.6) 1.76 (161.8)	2.0	1.47 (170.7) 1.56 (167.1) 1.71 (158.9)	2.67
6R	1.66 (174.7) 1.63 (176.6) 1.64 (175.5)	0.67	1.61 (166.0) 1.59 (173.4) 1.58 (171.1)	1.67	1.54 (160.5) 1.54 (171.9) 1.52 (167.9)	3.0

Fig. 5. The CH···O network of γ and δ′ phases at various pressures. The CH···O hydrogen bond is presented using a dashed blue line. The networks are becoming dense under compression. The criteria of the CH···O hydrogen bond are a bond length of <2.6 Å and a bond angle of >130°. The CH···O network of both phases became dense during compression.

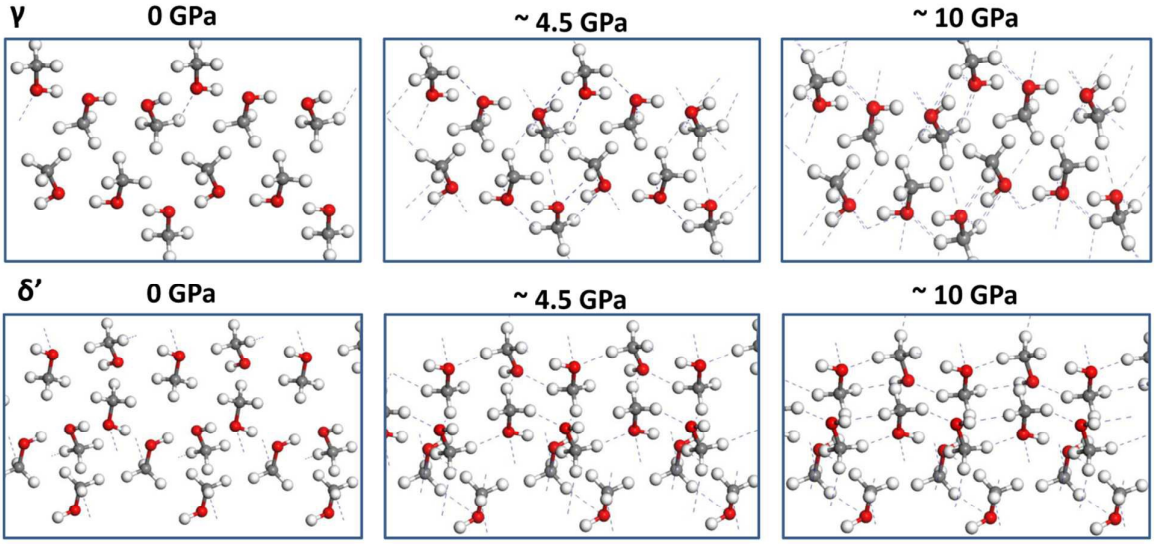

Fig. 6. Change in selected O···O distance (indicated by double-headed brown arrows) in 4S under compression. When pressure was applied on 4S, the side without the OH···O hydrogen bond was easily compressed. Subsequently, the O···O distance decreased sharply from 3.79 Å at 0 GPa to 3.51 Å at 4.5 GPa. When the pressure was >4.5 GPa, the O···O distance did not decrease considerably.

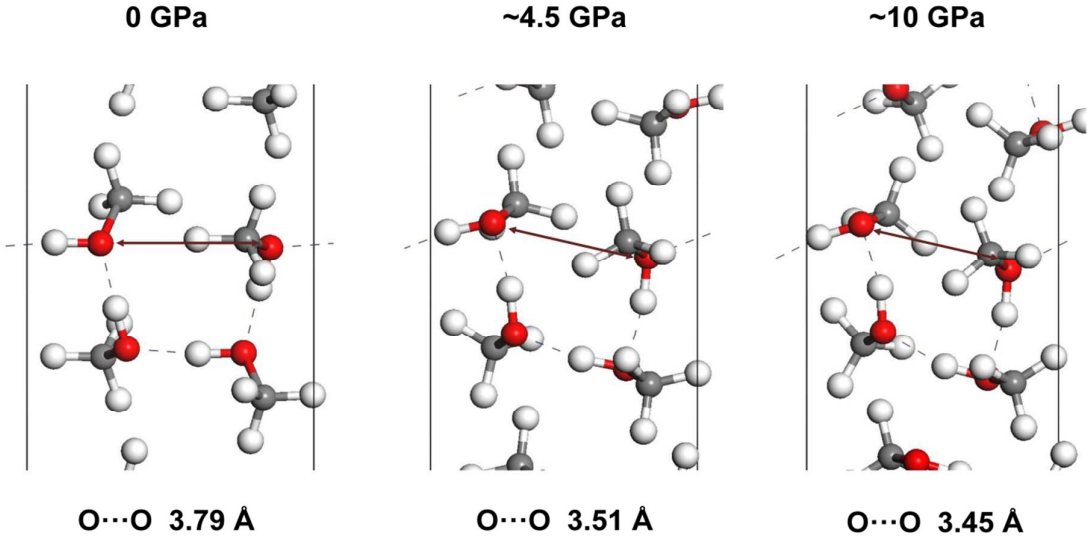

Fig. 7. Phase diagram of solid methanol based on the pressure–enthalpy curve in Fig. 4 and the dielectric measurement performed by Kondrin et al,[33] which is presented in Fig. S4. The red R represents all ring structures, namely 4R, 6R, and 4R2S. The gray area between the α and γ phases is provided because the relative enthalpy between these two phases is near this pressure range. Dashed lines for the β phase at 3 GPa and δ′ at 4 GPa are depicted because the structure maintained its form or transformed into other structures. 4S is indicated at the low temperature and pressure region of the β phase.